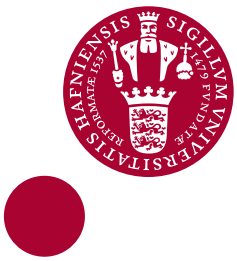

The Environment of the Binary Neutron Star Merger GW170817

Levan, A. J.; Lyman, J. D.; Tanvir, N. R.; Hjorth, J.; Mandel, I.; Stanway, E. R.; Steeghs, D.; Fruchter, A. S.; Troja, E.; Schroder, S. L.; Wiersema, K.; Bruun, S. H.; Cano, Z.; Cenko, S. B.; de Ugarte Postigo, A.; Evans, P.; Fairhurst, S.; Fox, O. D.; Fynbo, J. P. U.; Gompertz, B.; Greiner, J.; Im, M.; Izzo, L.; Jakobsson, P.; Kangas, T.; Khandrika, H. G.; Lien, A. Y.; Malesani, D.; O'Brien, P.; Osborne, J. P.; Palazzi, E.; Pian, E.; Perley, D. A.; Rosswog, S.; Ryan, R. E.; Schulze, S.; Sutton, P.; Thone, C. C.; Watson, D. J.; Wijers, R. A. M. J.

Published in:
Astrophysics Journal Letters

DOI:
10.3847/2041-8213/aa905f

Publication date:
2017

Document version
Publisher's PDF, also known as Version of record

The Astrophysical Journal Letters, 848:L28 (9pp), 2017 October 20 https://doi.org/10.3847/2041-8213/aa905f

The Environment of the Binary Neutron Star Merger GW170817

A. J. Levan[1], J. D. Lyman[1], N. R. Tanvir[2], J. Hjorth[3], I. Mandel[4], E. R. Stanway[1], D. Steeghs[1], A. S. Fruchter[5], E. Troja[6,7], S. L. Schrøder[3], K. Wiersema[2], S. H. Bruun[3], Z. Cano[8], S. B. Cenko[7,9], A. de Ugarte Postigo[3,8], P. Evans[2], S. Fairhurst[10], O. D. Fox[5], J. P. U. Fynbo[3], B. Gompertz[1], J. Greiner[11], M. Im[12,13], L. Izzo[8], P. Jakobsson[14], T. Kangas[5], H. G. Khandrika[5], A. Y. Lien[7,15], D. Malesani[3], P. O'Brien[2], J. P. Osborne[2], E. Palazzi[16], E. Pian[16], D. A. Perley[17], S. Rosswog[18], R. E. Ryan[5], S. Schulze[19], P. Sutton[10], C. C. Thöne[8], D. J. Watson[3], and R. A. M. J. Wijers[20]
[1] Department of Physics, University of Warwick, Coventry CV4 7AL, UK
[2] Department of Physics and Astronomy, University of Leicester, Leicester LE1 7RH, UK
[3] Dark Cosmology Centre, Niels Bohr Institute, University of Copenhagen, Juliane Maries Vej 30, 2100 Copenhagen Ø, Denmark
[4] Birmingham Institute for Gravitational Wave Astronomy and School of Physics and Astronomy, University of Birmingham, Birmingham B15 2TT, UK
[5] Space Telescope Science Institute, 3700 San Martin Drive, Baltimore, MD 21218, USA
[6] Department of Astronomy, University of Maryland, College Park, MD 20742-4111, USA
[7] Astrophysics Science Division, NASA Goddard Space Flight Center, 8800 Greenbelt Road, Greenbelt, MD 20771, USA
[8] Instituto de Astrofísica de Andalucía (IAA-CSIC), Glorieta de la Astronomía, s/n, E-18008 Granada, Spain
[9] Joint Space-Science Institute, University of Maryland, College Park, MD 20742, USA
[10] School of Physics and Astronomy, Cardiff University, Cardiff CF24 3AA, UK
[11] Max-Planck-Institut für extraterrestrische Physik, Giessenbachstr. 1, D-85740 Garching, Germany
[12] Center for the Exploration of the Origin of the universe (CEOU), Seoul National University, Seoul, Korea
[13] Astronomy Program, Department of Physics & Astronomy, Seoul National University, Seoul, Korea
[14] Centre for Astrophysics and Cosmology, Science Institute, University of Iceland, Dunhagi 5, 107 Reykjavík, Iceland
[15] Department of Physics, University of Maryland, Baltimore County, 1000 Hilltop Circle, Baltimore, MD 21250, USA
[16] INAF, Institute of Space Astrophysics and Cosmic Physics, Via Gobetti 101, I-40129 Bologna, Italy
[17] Astrophysics Research Institute, Liverpool John Moores University, IC2, Liverpool Science Park, 146 Brownlow Hill, Liverpool L3 5RF, UK
[18] The Oskar Klein Centre, Department of Astronomy, AlbaNova, Stockholm University, SE-106 91 Stockholm, Sweden
[19] Department of Particle Physics and Astrophysics, Weizmann Institute of Science, Rehovot 761000, Israel
[20] Anton Pannekoek Institute for Astronomy, University of Amsterdam, Postbus 94249, NL-1090 GE Amsterdam, The Netherlands
Received 2017 September 27; revised 2017 October 1; accepted 2017 October 2; published 2017 October 16

Abstract

We present *Hubble Space Telescope* (*HST*) and *Chandra* imaging, combined with Very Large Telescope MUSE integral field spectroscopy of the counterpart and host galaxy of the first binary neutron star merger detected via gravitational-wave emission by LIGO and Virgo, GW170817. The host galaxy, NGC 4993, is an S0 galaxy at $z = 0.009783$. There is evidence for large, face-on spiral shells in continuum imaging, and edge-on spiral features visible in nebular emission lines. This suggests that NGC 4993 has undergone a relatively recent ($\lesssim$1 Gyr) "dry" merger. This merger may provide the fuel for a weak active nucleus seen in *Chandra* imaging. At the location of the counterpart, *HST* imaging implies there is no globular or young stellar cluster, with a limit of a few thousand solar masses for any young system. The population in the vicinity is predominantly old with $\lesssim$1% of any light arising from a population with ages $<$500 Myr. Both the host galaxy properties and those of the transient location are consistent with the distributions seen for short-duration gamma-ray bursts, although the source position lies well within the effective radius ($r_e \sim 3$ kpc), providing an r_e-normalized offset that is closer than $\sim$90% of short GRBs. For the long delay time implied by the stellar population, this suggests that the kick velocity was significantly less than the galaxy escape velocity. We do not see any narrow host galaxy interstellar medium features within the counterpart spectrum, implying low extinction, and that the binary may lie in front of the bulk of the host galaxy.

Key words: galaxies: individual (NGC 4993) – galaxies: kinematics and dynamics – stars: neutron

1. Introduction

The existence of binary neutron stars that will eventually merge via the loss of angular momentum and energy through gravitational-wave (GW) emission has been recognized since the identification of the Hulse–Taylor pulsar (Hulse & Taylor 1975). These mergers have long been thought to manifest themselves as short-duration gamma-ray bursts (SGRBs; Eichler et al. 1989) and may produce additional optical/IR emission due to the synthesis of radioactive elements in their ejecta (e.g., Li & Paczyński 1998; Metzger & Berger 2012; Barnes & Kasen 2013). However, direct observations of confirmed neutron star mergers are challenging because smoking guns to their nature have been difficult to come by, and only in few cases have both signatures been reported (e.g., Berger et al. 2013; Tanvir et al. 2013).

This has changed with the discovery of GW170817, an unambiguous neutron star merger directly measured in gravitational waves (LIGO Scientific Collaboration & Virgo Collaboration 2017b), associated with an SGRB (LIGO Scientific Collaboration & Virgo Collaboration, Fermi-GBM & Integral 2017, in preparation) as well as a radioactively powered kilonova (e.g., LIGO Scientific Collaboration & Virgo Collaboration 2017, in preparation; Pian et al. 2017; Tanvir et al. 2017). For the first time this provides a route for studying the properties of a confirmed neutron star binary merger in

detail. In this Letter, we consider the environment of the merger, and the constraints this places on the properties of the progenitor binary.

2. Observations

GW170817 was detected by the advanced LIGO–Virgo observatory network on 2017 August 17:12:41:04 UT (LIGO Scientific Collaboration & Virgo Collaboration 2017b) and has a chirp consistent with a binary neutron star merger. Approximately 2 s later the *Fermi* Gamma-ray Burst Monitor (GBM) triggered on GRB 170817A (Connaughton et al. 2017; Goldstein et al. 2017a, 2017b; von Kienlin et al. 2017), as SGRB (duration $\sim$2 s) that was also seen by *INTEGRAL* (Savchenko et al. 2017). While the sky localizations of both events were large, they overlapped, and the combined spatial and temporal coincidence suggested causal association (LIGO Scientific Collaboration & Virgo Collaboration 2017, in preparation). Numerous groups undertook searches of the resulting GW-error region, revealing a counterpart in NGC 4993 (Coulter et al. 2017a, 2017b), independently confirmed by several groups (Allam et al. 2017; Arcavi et al. 2017; Lipunov et al. 2017; Tanvir & Levan 2017; Yang et al. 2017). The counterpart, known as SSS17a/AT 2017gfo, was seen to brighten in the IR and then dramatically redden in the following nights (Evans et al. 2017; Pian et al. 2017; Smartt et al. 2017; Tanvir et al. 2017), revealing broad features consistent with the expectations for a transient driven by heavy element (*r*-process) nucleosynthesis, often dubbed a kilonova (Li & Paczyński 1998; Metzger & Berger 2012; Barnes & Kasen 2013). These properties cement the association of the optical counterpart with both the GRB and the gravitational-wave trigger.

We obtained several epochs of ground- and space-based observations of the counterpart of GW170817. Observations with the Very Large Telescope using the MUSE integral field spectrograph were obtained on 2017 August 18. MUSE has a field of view of 1′ and covers the spectral range from 4800 to 9300 Å. Data were reduced using the ESO pipeline (v2.0.3) via `Reflex` and were fit for stellar continua and emission lines with IFUANAL as described in Lyman et al. (2017). *Hubble Space Telescope* (*HST*) observations were obtained between 2017 August 22 and 2017 August 28 in the F275W, F475W, F606W, F814W, F110W, and F160W filters via programmes GO 14804 (Levan), 14771 (Tanvir), and 14850 (Troja). A description of time variability of the counterpart in these images is provided in Tanvir et al. (2017). In addition, a single Advanced Camera for Surveys (ACS)/F606W observation of NGC 4993 was taken on 2017 April 28, prior to the discovery. Imaging observations were reduced via `astrodrizzle`, with the final scale set to 0.″025 (UVIS) and 0.″07 (IR). In addition, we analyze optical images (u, 2400 s; R, 240 s; z, 240 s) of NGC 4993 obtained at ESO with the Visible wide-field Imager and Multi-Object Spectrograph (VIMOS), on 2017 August 22, reduced via the standard `esorex` pipeline, and archival *Spitzer* observations, for which we used the processed, post-basic calibration (PBCD) data. A log of our observations and their times is given in Tanvir et al. (2017).

In addition, we also present *Chandra* observations of the host galaxy. A total of 47 ks were obtained on 2017 September 1 (program 18508587; PI: Troja). For analysis below we use a cleaned and extracted 0.5–8 keV image. Full details of the *Chandra* observations are given in Troja et al. (2017).

3. The Host Galaxy at Large

3.1. Morphology and Dynamics

At first sight, NGC 4993 appears to be a typical S0 galaxy: it has a strong bulge component and some visible dust lanes close to the galaxy core in the *HST* imaging (Figure 1), suggestive of recent merger activity in an ancient population. It has a measured redshift from our MUSE data of $z = 0.009783$, corresponding to a distance of 42.5 Mpc assuming a Hubble expansion with $H_0 = 69.6$ km s^{-1} and neglecting any peculiar velocity (see Hjorth et al. 2017 for further details of the distance to NGC 4993). Based on photometry in 1′ apertures, it has an absolute K-band magnitude of $M_K \sim -21.5$ (AB). A Sérsic fit to R-band and F606W images yields an effective radius of $\sim 16 \pm 1'' \approx 3$ kpc, with a Sérsic index of $n \sim 4$ that is indicative of a bulge/spheroid dominated galaxy. A fit to the global spectral energy distribution of the galaxy (see Table 1) suggests a stellar mass of $M_* \sim 1.4 \times 10^{11}\ M_\odot$ based on the stellar population models of Maraston (2005) and little to no ongoing star formation. These diagnostics are typically the only ones available for SGRB hosts, and indeed the properties of NGC 4993 are broadly in keeping with those of the fraction of massive early-type galaxies that host SGRBs (Fong et al. 2013, 2016). However, NGC 4993 is much closer than the host galaxies of all previously known SGRBs, making it possible to dissect it in greater detail, in particular with regard to its resolved morphology and the nature of the stellar population(s).

3.2. Stellar Populations

Stellar populations were fit to spaxel[21] bins across the host using STARLIGHT (Cid Fernandes et al. 2005) following the method detailed in Lyman et al. (2017). These provide spatially resolved maps[22] of stellar velocity, velocity dispersion, extinction, and ages for NGC 4993. Figure 3 shows the results of our fits. The galaxy is dominated by an older population with $>60\%$ of the mass arising from stars $\gtrsim 5$ Gyr in age in essentially all of the bins. In general, only 1%–2% of the light (and thus $\ll 1\%$ of the mass) in the best fits arises from stars with ages <500 Myr. The strong Balmer absorption and lack of evidence for young stellar populations is reminiscent of post-starburst or post-merger galaxy spectra. This is borne out in our fits, which indicate a strong contribution from an intermediate ($\sim$ Gyr) stellar population that may be responsible for the ionized gas we see (see Section 3.3 and Figure 4) via post-AGB stars.

For galaxies such as this, it is unsurprising that a single population does not provide a good fit to the resulting data. However, including large numbers of model population ages in the fit, which contribute progressively less light, risks over-interpreting the data or systematics within it and are increasingly prone to degenerate fits. We use a relatively sparse number of model ages (13) and find that repeat fitting with just six ages gave similar results. The contribution of the young stellar population disappears in a large fraction of the bins using the reduced model set, indicating that they contribute no more than 1%–2% of the light.

[21] A spaxel is a spectral pixel in an integral field spectrograph, where each spatial pixel provides spectral coverage.

[22] Spaxel bins used a Voronoi binning algorithm to achieve a minimum signal-to-noise ratio of 25 (Cappellari & Copin 2003) and remain $\lesssim 1''$ in radius, even in the fainter outskirts of the host.

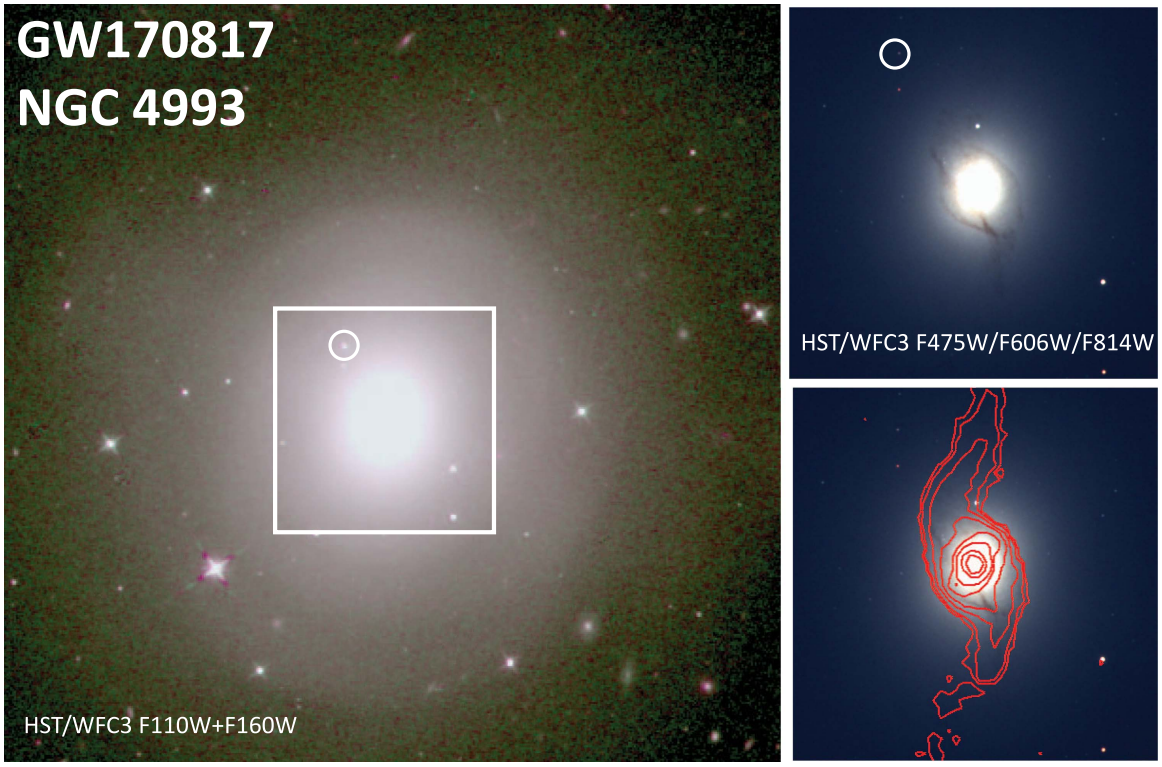

Figure 1. Imaging of the host galaxy of GW170817 with *HST*. The left panel shows the galaxy observed in the IR with F110W and F160W, where the counterpart is marked with a circle. The top right panel shows the zoomed-in region observed with WFC3/UVIS, demonstrated the presence of strong dust lanes in the inner regions. The bottom right panel shows the same image, but with the MUSE contours in the [N II] line superimposed, showing the strong spiral features that only appear in the emission lines. Some of these features appear to trace the dust lanes.

Table 1
Photometry of NGC 4993

Instrument	Band	Magnitude (AB)
HST/WFC3	F275W	19.87 ± 0.15
VLT/VIMOS	*U*	14.96 ± 0.01
VLT/VIMOS	*R*	12.13 ± 0.01
VLT/VIMOS	*z*	11.60 ± 0.01
HST/WFC3	F110W	11.27 ± 0.01
HST/WFC3	F160W	10.94 ± 0.01
VLT/HAWK-I	*K*	11.50 ± 0.01
Spitzer/IRAC	3.6 μm	11.81 ± 0.02
Spitzer/IRAC	4.5 μm	12.34 ± 0.02

Note. Photometry has been measured in 1′ apertures centered on the host galaxy, and bright foreground stars have been masked from the image (except for F275W where a smaller aperture was used due both to the centrally concentrated nature of the UV emission and the windowed WFC3 FOV). The errors given are statistical only. Given the uncertainty introduced by the masking, and possible low surface brightness features it is reasonable to assume systematics of ∼0.1 mag. Magnitudes have not been corrected for foreground extinction.

3.3. Evidence for Past Merger and Emission Line Properties

Chandra X-ray observations reveal a compact source consistent (±0.″5) with the nucleus of the galaxy, with a luminosity (for a photon index of $\Gamma = 2$) of $L_X \approx 2 \times 10^{39}$ erg s^{-1} (0.5–8 keV). There is no obvious extended emission associated with features seen at other wavelengths, although further point sources in the vicinity may be associated with NGC 4993. This X-ray emission is most likely due to a weak active galactic nucleus (AGN), in keeping with a 0.4 mJy radio detection at 19 GHz (Troja et al. 2017). At large scales the velocity dispersion within the effective radius within our MUSE cube is ∼170 km s^{-1}, and this yields a black hole mass from $M_{\rm BH} - \sigma$ relations (Ferrarese & Merritt 2000; Gültekin et al. 2009) of $M_{\rm BH} \approx 10^8\ M_\odot$. For this black hole mass the AGN is only accreting at $\sim 10^{-6}$ of the Eddington luminosity.

Face-on spiral shell-like features can be seen extending to large radii (∼1′ or 12 kpc) in our *HST* imaging. Emission line fits were attempted within the MUSE cube throughout the host after subtraction of the underlying stellar continuum. Ionized gas can be seen in spiral arms with a relatively strong (∼0.8 kpc) bar (see Figures 1 and 4). Notably, these spiral features seen in nebular emission lines appear with a high ratio of minor to major axes, suggesting an almost edge-on alignment. The velocity structure in these edge-on spiral arms extends to ∼220 km s^{-1} within the central kiloparsec of the galaxy, while the stellar components appear to be dominated by much lower velocities (∼100 km s^{-1}; Figure 3). Furthermore, the large-scale spiral arms/shells are almost circular (and hence face-on), while the spiral features seen in emission lines are near edge-on. The decoupled dynamics of the gas and stars suggest a relatively recent merger, and that the galaxy has not yet relaxed. This would also be consistent with the presence of dust lanes in a quiescent galaxy (e.g., Kaviraj et al. 2012; Shabala et al. 2012), as seen in our *HST* optical imaging (see Figure 1). This recent merger would provide the natural fuel to power nuclear accretion.

The presence of extended emission lines could imply star formation in the host galaxy; however, the emission line ratios are difficult to explain with photoionization from young stars. We find [N II] λ6583/Hα (and [O III] λ5007/Hβ, where it could be measured) ratios of ∼1 (Figure 4). Such ratios are

typical of those seen in AGNs and low-ionization nuclear emission line regions (LINERs). However, the relative weakness of any AGN, combined the large spatial extent of these lines and their spiral structure is very different to typical extended emission line regions seen around some AGN. We therefore conclude that AGN power is not responsible for their creation. Instead, these features are similar to the so-called LIER regions (non-nuclear LINER regions) that have been found in other early-type galaxies without AGN activity (Sarzi et al. 2010; Singh et al. 2013). These may be driven by intermediate-aged stellar populations (e.g., hot post-AGB stars) or shocks. Since these emission lines are not excited by young stars associated with recent star formation, they cannot be used to reliably derive a gas-phase metallicity for the galaxy.

4. At the Transient Location

Our imaging shows the transient is located at position offset $8\farcs92$ N and $5\farcs18$ E of the host galaxy centroid, with a total projected offset of $10\farcs31 \pm 0\farcs01$, corresponding to 1.96 kpc offset at a 40 Mpc distance.[23] Our observations provide constraints on the immediate environment of the transient and on any underlying source.

4.1. In Emission

Any source underlying the transient position is of significant interest since it could indicate either a young stellar cluster (and hence young progenitor) or a globular cluster in which the neutron star–neutron star (NS–NS) binary may have formed dynamically (Grindlay et al. 2006). At the location of the transient in the F606W imaging obtained prior to GW170817 (see also Foley et al. 2017) we place a 2σ upper limit on any point source by subtracting an isophotal fit to the smooth light of the galaxy and then by performing aperture photometry on the galaxy subtracted image. The resulting point-source limit is F606W > 26.4 (2σ), corresponding to an absolute magnitude of $M_V > -6.7$ (note that at 40 Mpc globular clusters should appear point-like as the *HST* point-spread function (PSF) is $\sim$20 pc; indeed point sources in the images around the galaxy have colors consistent with globular clusters associated with NGC 4993). This is well down the globular cluster luminosity function and only $\sim$30% of Milky Way globular clusters would evade detection at this limit (Harris 1996). However, clusters fainter than this limit only contain $\sim$5% of the stellar mass in globular clusters. We consider the implications of this further in Section 5.

There is no detection of the counterpart in F275W images taken on 2017 August 25 and 2017 August 28 (see Troja et al. 2017). Hence, in addition to constraining the counterpart, they can also place limits on underlying young populations. Combining two epochs of F275W observations (exposure time of 1240 s) places a limit on the UV luminosity of any source of F275W > 26.0 (2σ, AB), corresponding to an absolute magnitude limit of F275W(AB) $\gtrsim -7$. This absolute magnitude limit is comparable to the UV absolute magnitudes of massive O-stars or Wolf–Rayet stars and suggests little underlying star formation. Indeed, combined with the optical limit from pre-imaging, this indicates that any underlying young (10^7–10^8 years) star cluster could have a mass of only a few thousand solar masses (based on the BPASS models of Eldridge et al. 2017).

Given the lack of any point source, we can characterize the location of the transient relative to the host galaxy light, defining the fraction of surface brightness contained in pixels of equal or lower surface brightness to the pixel hosting the transient, the so-called $F_{\rm light}$ parameter (Fruchter et al. 2006). This statistic is complicated in this case by the extended low surface brightness features and the presence of foreground stars projected onto the galaxy. Masking these stars and considering light within a large ($1'$ radius) aperture suggests that $F_{\rm light} \approx 0.6$. This is at the upper end of those seen in SGRBs (Fong & Berger 2013), although it should be noted that in SGRBs at higher redshift, cosmological surface brightness dimming could result in the omission of low surface brightness features in the comparison samples. The loss of light at low surface brightness (compared to the transient position) would lower the value of $F_{\rm light}$. Alternatively, one can consider the host normalized offset (the offset of the transient from its host nucleus in units of the effective radius), which in this instance is also $\sim$0.6, smaller than the typical SGRB offsets (Fong & Berger 2013). While these values are consistent with the distributions seen for SGRBs, the location of GW170817 within its host galaxy is comparable to the most centrally concentrated 10% of SGRBs.

4.2. In Absorption

We searched for narrow absorption features in the transient spectrum obtained with MUSE, but did not find any convincing examples. The transient's features are too broad to be useful for velocity measurements, especially since their identification is uncertain. Hence, the velocity of the source relative to the host galaxy cannot be directly determined.

Notably, the region around the counterpart shows evidence for modest extinction of $E(B-V) = 0.07$ mag based on the stellar population fits (see Figure 2), assuming an $R_V = 3.1$ extinction law. If the extinction directly underlying the transient position is the same, then in principle this should be visible as Na I D absorption in the counterpart spectrum, the equivalent width of which can be calculated from established relations (Poznanski et al. 2012). Indeed, this doublet is seen in the sole SGRB spectrum to show absorption features in its afterglow (de Ugarte Postigo et al. 2014). The expected lines for $E(B-V) = 0.07$ mag are shown in Figure 2, where we have subtracted a scaled version of the annulus spectrum in order to correct the transient spectrum for the Na I D absorption that arises from a stellar origin within the transient aperture, with the shaded region demonstrating the 1σ scatter in this relation. There is no evidence for such absorption. The absence of interstellar medium (ISM) absorption in the counterpart spectrum could imply that the transient emission may lie in front of the stellar population (or gas) in the galaxy. This may be because it is naturally located within the halo population, or alternatively could be indicative that the progenitor received a kick that has placed it outside the bulk of the stellar population. Ultimately, a re-observation of the explosion site, once the transient has faded, will allow us to investigate this further by directly measuring the extinction to the stellar population under the transient position. However, since the extinction measured in the annulus around the transient is typical of extinction across the galaxy (see the top right panel of Figure 3), our value seems reasonable.

[23] This provides a lower limit on the true offset since we cannot measure the source location relative to its host along our line on sight.

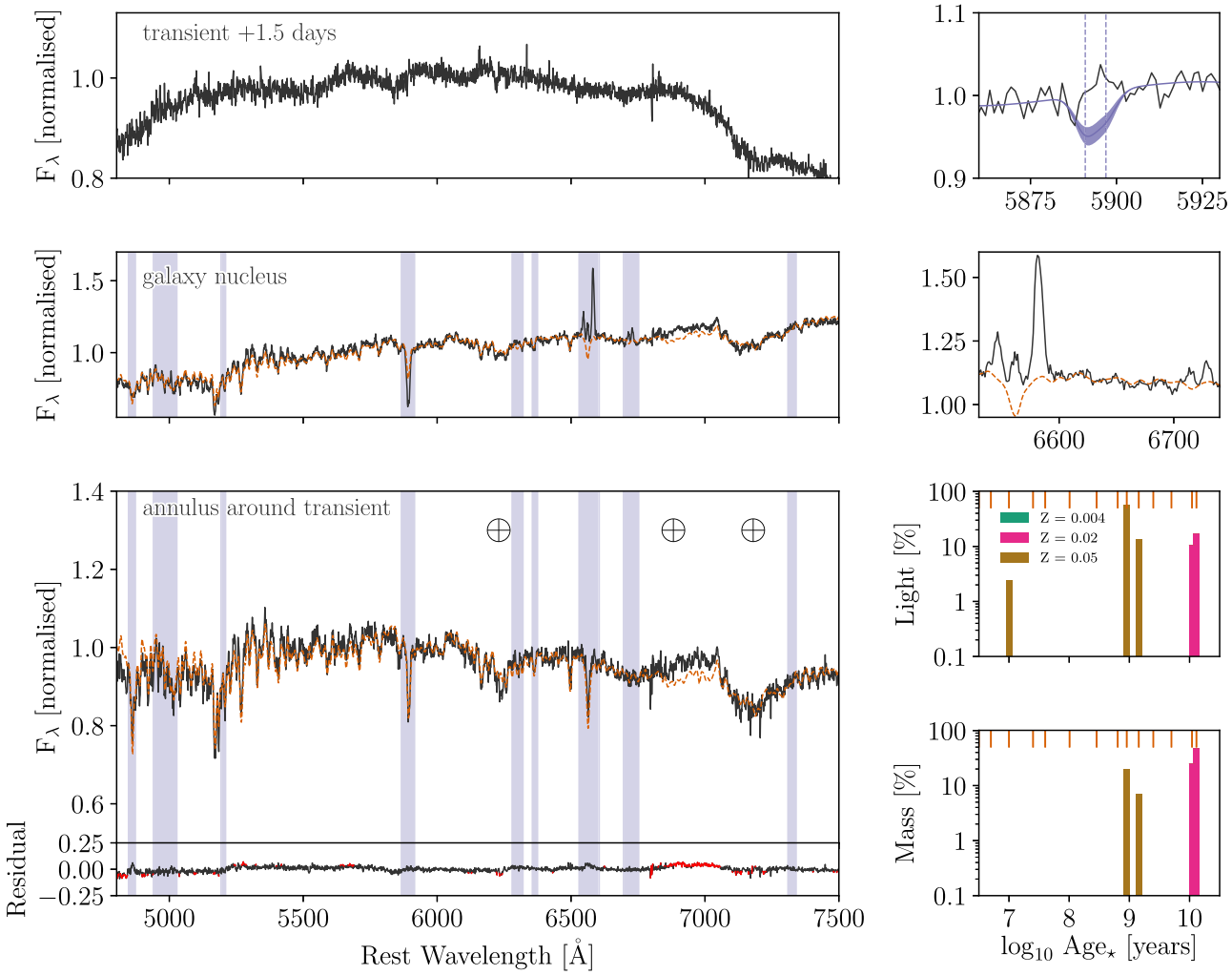

Figure 2. Bottom: stellar population results in an annulus 1.″5–2″ around the transient. The extracted MUSE spectrum (black) with model continuum fit (orange dashed) and residuals (lower panel). Wavelengths clipped are indicated in red in the residual panel and largely coincide with regions of telluric features (indicated on fit panel). Shaded regions are masked from the fit. The light and mass contribution of the stellar population models by age (abscissa) and metallicity by mass fraction (color) to the total fit are shown on the right. Orange tick marks (top axis) indicate the ages of all models used in the fit. The small contribution of the 10 Myr stellar population is not robust to varying the model set used. We consider it an upper estimate of any young stellar population contribution. The best-fit extinction is $A_V = 0.22$ mag. Middle: stellar population fit for the nucleus of NGC 4993. The conspicuous emission lines of Hα, [N II], and [S II] are shown in a zoomed-in panel on the right. Top: a 0.″4 radius aperture extracted at the transient location after subtracting the annulus spectrum (scaled by the ratio of the area of the aperture and annulus). The right panel shows a zoom-in around Na I $\lambda\lambda$5890, 5896. Overlaid on the transient spectrum is the Na I absorption expected based on the extinction derived in the annulus, using the equivalent width relations of Poznanski et al. (2012; see the text) with a 1σ shaded region. The absorption was simply modeled as two Gaussians with $\sigma = \sigma_\star$(annulus) plus a low-order polynomial to fit the continuum. All spectra are normalized to the flux in the range 5590–5680 Å.

5. Comparison with Expectations from Binary Evolution

The location of a binary neutron star merger depends on its initial location, the delay time between the formation of the second NS and the merger, the kick given to the binary at the time of NS formation, and the galactic potential in which the system moves.

Within the Milky Way, the majority of binary neutron stars are formed in the field through isolated binary evolution, while a single example exists in a globular cluster, likely formed via dynamical interactions (Anderson et al. 1990), and similar interactions may produce a significant fraction of extragalactic systems (Grindlay et al. 2006).

There is no evidence in our data supporting the dynamical formation scenario. The closest point-like sources in the stellar field of the galaxy are approximately 2.″5 from the transient location, corresponding to an offset of ∼500 pc (a lower limit owing to projection effects). The absence of a globular cluster at the transient location strongly disfavors a merger within a globular cluster. Dynamical formation involves a sequence of three-body (2+1) interactions that leave more massive stars within tighter binaries (Davies 1995). The rate of these interactions scales roughly as $L^{3/2}/r^{5/2}$ (Bregman et al. 2005), indicating that massive, core-collapsed systems disproportionately dominate the interaction rate (Davies & Benz 1995). In this sense, the faintest 30% of globular clusters contain 5% of the mass in globular clusters, but probably have $\ll$5% of the interactions, indicating a very low probability of an underlying cluster creating the binary that formed GW170817. However, two caveats apply to this. First, if a significant population of black holes remains in the cluster, the more massive black holes will substitute into compact binaries during 2+1 interactions and black hole–black (BH–BH) binaries would be formed at the expense of NS–NS binaries (e.g., Rodriguez et al. 2016). Second, interactions can eject the binaries given the low escape velocities of globular clusters.

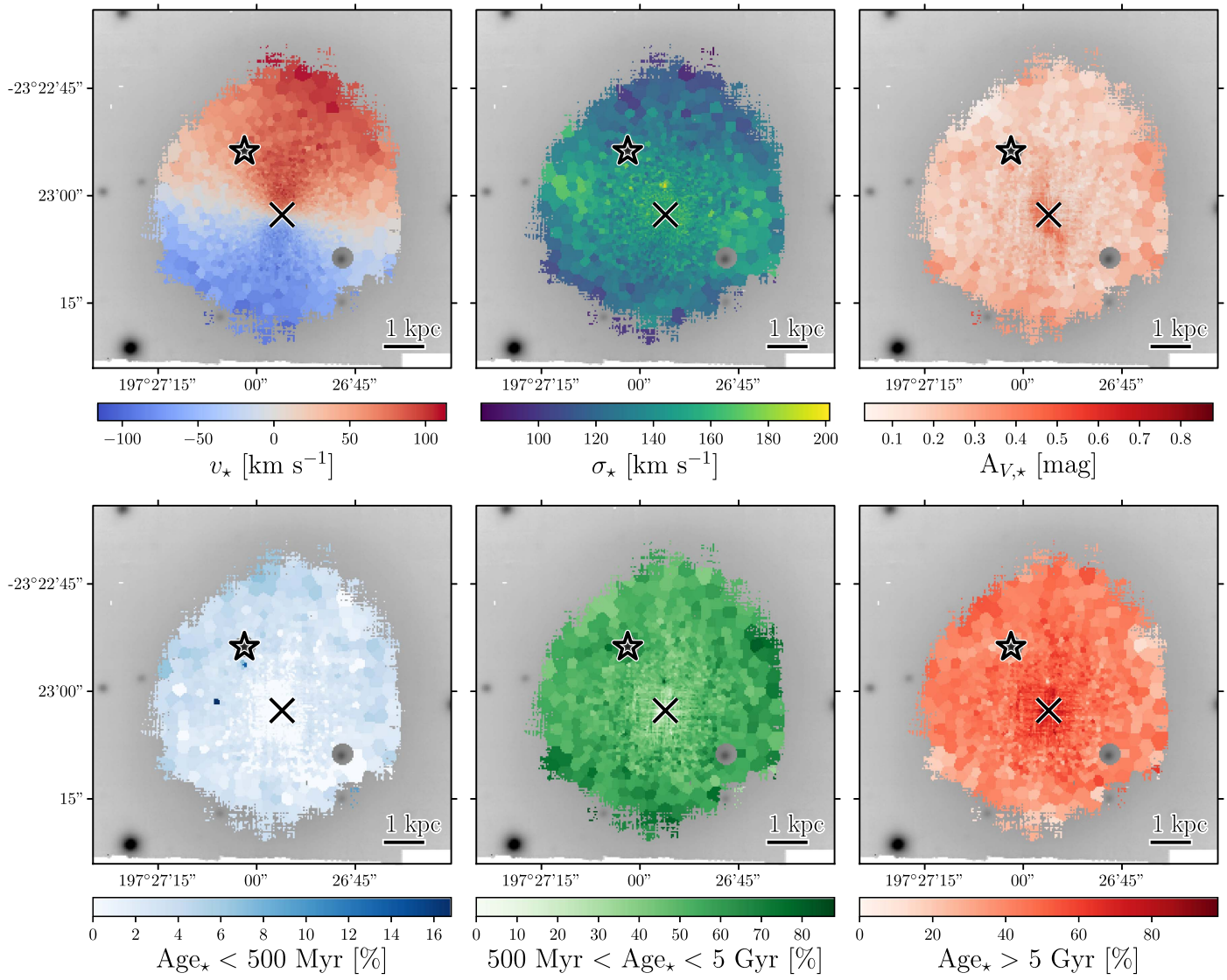

Figure 3. Voronoi binned stellar population property maps of NGC 4993 from our stellar continuum fitting. Top row: stellar velocity offset relative to the galaxy nucleus (left), stellar velocity dispersion (middle), and visual extinction (right). Bottom row: the flux contribution to the best-fit continuum model for young (left), intermediate (middle), and old (right) stellar populations; the age divisions are indicated on the respective color bars. The galaxy nucleus and transient locations are indicated by cross and star symbols, respectively. North is up, east is left, and the linear scale at a distance of 40 Mpc is shown. Maps are overlaid on a collapsed view of the MUSE data cube. Masks (gray circles) have been applied around the transient and a foreground star.

With modest velocities and long delay times these may be indistinguishable from field systems based on their locations, although it may be possible to distinguish field and dynamically formed binaries based on their intrinsic properties (masses, spins, etc.) measured from the gravitational waves themselves (e.g., Farr et al. 2017; Stevenson et al. 2017; Zevin et al. 2017).

The absence of any significant young population within the galaxy, or of young stars underneath the burst position, suggests that the progenitor of GW170817 was likely old ($>10^9$ years). This old age is consistent with the ages of Milky Way double neutron star systems (e.g., Tauris et al. 2017). However, rapidly merging systems are observationally selected against (because they merge quickly, the time when they are detectable is short), and some population syntheses suggest that a significant fraction could have very short delay times if the progenitor of the second-born neutron star either enters a second common envelope phase after the helium main sequence (Dewi & Pols 2003) or stably transfers a significant amount of mass that is then lost from the binary (e.g., Belczynski et al. 2006; Eldridge & Stanway 2016; van den Heuvel et al. 2017).

The delay times for some of these models are $\sim 10^6$ years or less (Belczynski et al. 2006), and so binaries could not travel far from their birth location. The absence of any underlying cluster or point source close to the transient position can therefore offer information on the likelihood of a very short delay progenitor. First, it is unlikely that a low-mass cluster would be present close to the transient position without other signs of star formation more widely distributed in the host galaxy. Second, such a low-mass cluster would be unlikely to form many massive stars. For a typical initial mass function (e.g., Kroupa & Weidner 2003), a 1000 $M_\odot$ cluster would be expected to form $\sim$10 stars capable of forming supernovae. Since $\lesssim$10 merging binary neutron stars are expected to form per million solar masses of star formation (Abadie et al. 2010), the probability of obtaining such a binary from a single low-mass star-forming region is very small.

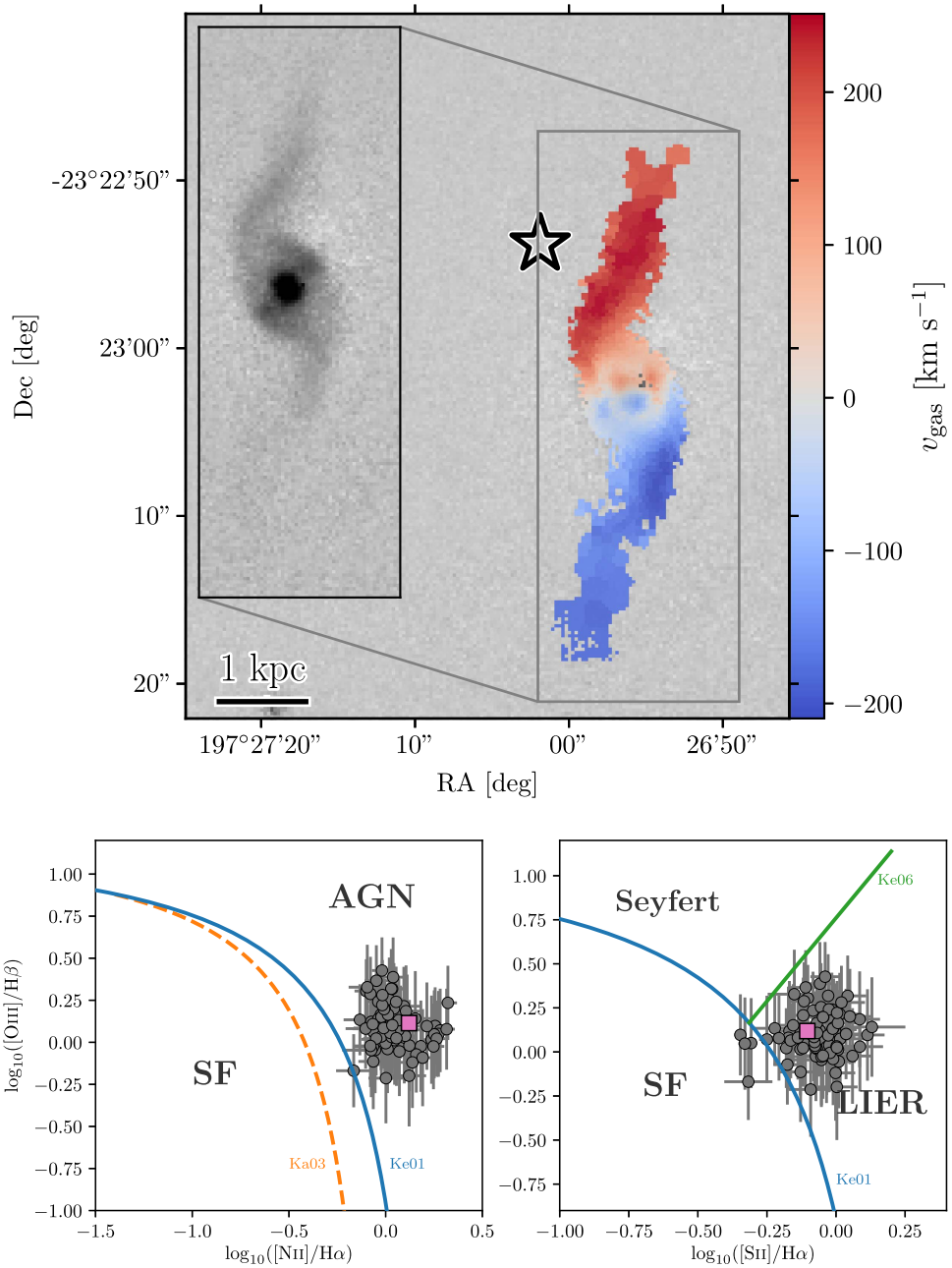

Figure 4. Top: velocity map of ionized gas in NGC 4993. Velocities are the offsets of [N II] λ6583 emission. The location of the transient is indicated with a star symbol. Inset shows an [N II] λ6583 narrowband image constructed from the MUSE data cube. The motion of the "arm"-like features is in the radial velocity plane, implying they are edge-on. Bottom: emission line ratios in NGC 4993. Each point represents a spaxel bin where all the diagnostic lines are detected as a signal-to-noise ratio of >2. Dividing lines of Kauffmann et al. (2003; pure star formation, orange dashed), Kewley et al. (2001a; theoretical star formation limit, blue) and Kewley et al. (2001b; Seyfert vs. LIER, green) are shown. The ionized gas regions in NGC 4993 are inconsistent with being driven by star formation (SF) and are better described as extended LIERs (see Sarzi et al. 2010; Singh et al. 2013). The few bins formally within theoretical SF limits show velocity dispersions $\sigma_{\rm gas} > 100$ km s^{-1}, inconsistent with typical H II regions that show tens of km s^{-1}. The position of the integrated emission lines (summing all bins) is shown by a square on each plot.

Observations of a single object cannot provide a delay time distribution for a binary population, but they do demonstrate on this occasion that the delay time was large.

The question of the kick velocity is even more difficult to determine. The space velocity of a binary neutron star relative to the initial velocity of its center of mass in the galactic potential is set by the kick imparted at each supernova. Such a kick has two contributing factors, the natal kick to the neutron star and the mass-loss kick from the binary. The majority of binaries are disrupted during one of the supernova events; only those for which the mass loss is small, and the natal kick is fortuitous in direction, are likely to survive. For this reason it is likely that the binary neutron star population has slower velocities than isolated pulsars, and there is evidence to suggest this is true (Dewi & Pols 2003).

Once kicked, binaries move in the gravitational potential of their host galaxy. For high-velocity kicks they may be ejected completely or move on highly elliptical orbits. For weak kicks, they may orbit much closer to the galaxy and may oscillate around the radius at which they were formed. We quantify this

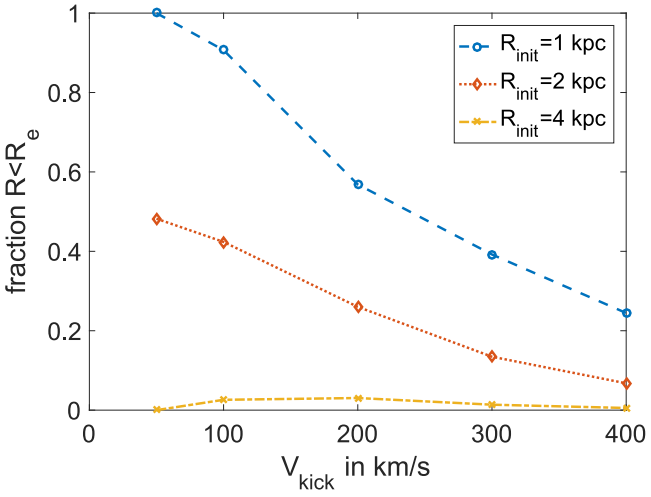

Figure 5. Fraction of time that a binary with a given kick velocity magnitude spends within $R_e = 2$ kpc of the galactic center. Binaries are assumed to form on circular orbits around the galactic center at initial distances of 1 kpc (blue), 2 kpc (orange), or 4 kpc (yellow) from the center. For formation at 4 kpc from the center and kicks of 400 km s^{-1}, 7% of binaries are unbound; these are not included in the plot. All other simulated binaries are bound, and the plot is reflective of the merger location if the delay time between double compact object formation and gravitational-wave driven merger is longer than the dynamical timescale.

in Figure 5, where we show binaries kicked isotropically at different velocities from circular orbits at three initial radii within the host galaxy. Once kicked, these binaries are assumed to move in the gravitational potential equal to the Milky Way potential model of Irrgang et al. (2013) with the disk removed. As a bulge-dominated lenticular galaxy there is little, if any, disk component in NGC 4993, and this model provides a good description of the rotational velocities seen in Figure 4. For long delay times ($\gg$ orbital period of the binary around the galaxy), the probability of merging beyond a given radius (for example, the effective radius) is equal to the fraction of time the binary spends beyond this radius.

As indicated in Figure 5, a strongly kicked binary with a long delay time is likely to be found at radii outside the effective radius, whatever its initial location. Indeed, the presence of the counterpart of GW170817 relatively close to the center of the host would favor a small kick if the system is old, as our stellar population analysis suggests. As with the issue of delay times, a single event provides little information as to the properties of the population, but it is worth noting that the proximity of GW170817 to its host would place it among the most centrally concentrated $\sim$10% of SGRBs (e.g., Fong & Berger 2013). This may suggest that the kick in GW170817 was unusually small, that it was directed toward us (minimizing the projected offset), or that a binary in a more extended orbit happened to merge when passing relatively close to the core of its host galaxy.

6. Summary and Conclusions

We have presented comprehensive imaging and integral field spectroscopy of the host galaxy and local environment of the first electromagnetic counterpart to a gravitational-wave source. These observations provide a unique view of the regions around this event, and its properties are consistent with those seen in the population of SGRB hosts. We find a highly inclined ionized gas disk that is kinematically decoupled from the stellar velocity field, as well as extended face-on arm/shell features in the stellar light profile. These indicate the galaxy has undergone a major merger relatively recently. We find that $\sim$20% of the galaxy, by mass, is $\sim$1 Gyr old, perhaps as a result of this merger, while most of the remaining mass is $>$5 Gyr old. There is minimal contribution (if any) from a young stellar population ($\ll$1% of the mass), implying an old ($\gtrsim$Gyr) progenitor. The absence of absorption features in the counterpart spectrum and moderate extinction of the stellar population in the vicinity of the transient source offer tentative evidence that it lies on the near side of the galaxy, either by chance or due to a kick in our direction.

Galaxy demographics and population synthesis have previously been used to argue for the origin of SGRBs in compact object mergers. Since this scenario now seems secure the direction of inference can now be reversed, and the properties and locations of SGRBs and gravitational-wave sources can be used to pinpoint the details of extreme stellar evolution that lead to the formation of compact object binaries.

We thank the referee for a prompt and highly constructive report that improved the content and clarity of the manuscript. We also thank the editor, Fred Rasio, for helpful comments. Based on observations made with ESO Telescopes at the La Silla Paranal Observatory under programme ID 099.D-0668 (A.J.L.), and on observations made with the NASA/ESA *Hubble Space Telescope*, obtained from the data archive at the Space Telescope Science Institute. STScI is operated by the Association of Universities for Research in Astronomy, Inc. under NASA contract NAS 5-26555. These observations are associated with programs GO 14771 (N.R.T.), GO 14804 (A.J.L.), and GO 14850 (E.T.). We thank the staff at ESO and STScI for their excellent support of these observations. A.J.L. acknowledges that this project has received funding from the European Research Council (ERC) under the European Union's Horizon 2020 research and innovation programme (grant agreement No. 725246) A.J.L., D.S., and J.D.L. acknowledge support from STFC via grant ST/P000495/1. N.R.T., K.W., P.T.O., J.L.O., and S.R. acknowledge support from STFC. J.H. was supported by a VILLUM FONDEN Investigator grant (project number 16599). A.d.U.P., C.T., Z.C., and D.A.K. acknowledge support from the Spanish project AYA 2014-58381-P. Z.C. also acknowledges support from the Juan de la Cierva Incorporación fellowship IJCI-2014-21669, and D.A.K. from Juan de la Cierva Incorporación fellowship IJCI-2015-26153. M.I. was supported by the NRFK grant, No. 2017R1A3A3001362. E.T. acknowledges support from grants GO718062A and HSTG014850001A. S.R. has been supported by the Swedish Research Council (VR) under grant number 2016-03657_3, by the Swedish National Space Board under grant number Dnr. 107/16 and by the research environment grant "Gravitational Radiation and Electromagnetic Astrophysical Transients (GREAT)" funded by the Swedish Research council (VR) under Dnr 2016-06012. P.A.E. acknowledges UKSA support.

Facilities: Hubble Space Telescope, Very Large Telescope.

Software: Numpy, PyRAF, ASTROPY (Astropy Collaboration 2013), STARLIGHT (Cid Fernandes et al. 2005), REFLEX (Freudling et al. 2013).

ORCID iDs

A. J. Levan https://orcid.org/0000-0001-7821-9369
N. R. Tanvir https://orcid.org/0000-0003-3274-6336

J. Hjorth https://orcid.org/0000-0002-4571-2306
E. R. Stanway https://orcid.org/0000-0002-8770-809X
Z. Cano https://orcid.org/0000-0001-9509-3825
S. B. Cenko https://orcid.org/0000-0003-1673-970X
S. Fairhurst https://orcid.org/0000-0001-8480-1961
O. D. Fox https://orcid.org/0000-0003-2238-1572
D. Malesani https://orcid.org/0000-0002-7517-326X
E. Pian https://orcid.org/0000-0001-8646-4858
D. A. Perley https://orcid.org/0000-0001-8472-1996
D. J. Watson https://orcid.org/0000-0002-4465-8264

References

Abadie, J., Abbott, B. P., Abbott, R., et al. 2010, CQGra, 27, 173001
Allam, I., et al. 2017, GCN, 21530
Anderson, S. B., Gorham, P. W., Kulkarni, S. R., Prince, T. A., & Wolszczan, A. 1990, Natur, 346, 42
Arcavi, I., et al. 2017, GCN, 21538
Astropy Collaboration 2013, A&A, 558, 33
Barnes, J., & Kasen, D. 2013, ApJ, 775, 18
Belczynski, K., Perna, R., Bulik, T., et al. 2006, ApJ, 648, 1110
Berger, E., Fong, W., & Chornock, R. 2013, ApJL, 774, L23
Bregman, J. N., Miller, E. D., Athey, A. E., & Irwin, J. A. 2005, ApJ, 635, 1031
Cappellari, M., & Copin, Y. 2003, MNRAS, 342, 345
Cid Fernandes, R., Mateus, A., Sodré, L., Stasińska, G., & Gomes, J. M. 2005, MNRAS, 358, 363
Connaughton, V., Blackburn, L., Briggs, M., et al. 2017, GCN, 21506
Coulter, D. A., et al. 2017a, GCN, 21529
Coulter, D. A., Kilpatrick, C. D., Siebert, M. A., et al. 2017b, Sci, https://doi.org/10.1126/science.aap9811
Davies, M. B. 1995, MNRAS, 276, 887
Davies, M. B., & Benz, W. 1995, MNRAS, 276, 876
de Ugarte Postigo, A., Thöne, C. C., Rowlinson, A., et al. 2014, A&A, 563, A62
Dewi, J. D. M., & Pols, O. R. 2003, MNRAS, 344, 629
Eichler, D., Livio, M., Piran, T., & Schramm, D. N. 1989, Natur, 340, 126
Eldridge, J. J., et al. 2017, PASA, submitted
Eldridge, J. J., & Stanway, E. R. 2016, MNRAS, 462, 3302
Evans, P., Cenko, S., Kennea, D. A., et al. 2017, Sci, https://doi.org/10.1126/science.aap9580
Farr, W., Stevenson, S., Miller, M. C., et al. 2017, Natur, 548, 426
Ferrarese, L., & Merritt, D. 2000, ApJL, 539, L9
Foley, R. J., Kilpatrick, C. D., Nicholl, M., & Berger, E. 2017, GCN, 21536
Fong, W., & Berger, E. 2013, ApJ, 776, 18
Fong, W., Berger, E., Chornock, R., et al. 2013, ApJ, 769, 56
Fong, W., Margutti, R., Chornock, R., et al. 2016, ApJ, 833, 151
Freudling, W., Romaniello, M., Bramich, D. M., et al. 2013, A&A, 559, 96
Fruchter, A. S., Levan, A. J., Strolger, L., et al. 2006, Natur, 441, 463
Goldstein, A., Veres, P., Burns, E., et al. 2017a, ApJL, https://doi.org/10.3847/2041-8213/aa8f41
Goldstein, A., Veres, P., von Kienlin, A., et al. 2017b, GCN, 21528
Grindlay, J., Portegies Zwart, S., & McMillan, S. 2006, NatPh, 2, 116
Gültekin, K., Richstone, D. O., Gebhardt, K., et al. 2009, ApJ, 698, 198
Harris, W. E. 1996, AJ, 112, 1487
Hjorth, J., Levan, A., Tanvir, N., et al. 2017, ApJL, https://doi.org/10.3847/2041-8213/aa9110
Hulse, R. A., & Taylor, J. H. 1975, ApJL, 195, L51
Irrgang, A., Wilcox, B., Tucker, E., & Schiefelbein, L. 2013, A&A, 549, A137
Kauffmann, G., Heckman, T. M., Tremonti, C., et al. 2003, MNRAS, 346, 1055
Kaviraj, S., Crockett, R. M., Whitmore, B. C., et al. 2012, MNRAS, 422, L96
Kewley, L. J., Dopita, M. A., Sutherland, R. S., et al. 2001a, ApJ, 556, 121
Kewley, L. J., Groves, B., Kauffmannm, G., & Heckman, T. 2001b, ApJ, 556, 121
Kroupa, P., & Weidner, C. 2003, ApJ, 598, 1076
Li, L.-X., & Paczyński, B. 1998, ApJL, 507, L59
LIGO Scientific Collaboration & Virgo Collaboration 2017a, GCN, 21509
LIGO Scientific Collaboration & Virgo Collaboration 2017b, PhRvL, https://doi.org/10.1103/PhysRevLett.119.161101
Lipunov, V., et al. 2017, GCN, 21546
Lyman, J. D., Taddia, F., Stritzinger, M. D., et al. 2017, MNRAS, in press (arXiv:1707.04270)
Maraston, C. 2005, MNRAS, 362, 799
Metzger, B. D., & Berger, E. 2012, ApJ, 746, 48
Pian, E., D'Avanzo, P., Benetti, S., et al. 2017, Natur, https://doi.org/10.1038/nature24298
Poznanski, D., Prochaska, J. X., & Bloom, J. S. 2012, MNRAS, 426, 1465
Rodriguez, C. L., Chatterjee, S., & Rasio, F. A. 2016, PhRvD, 93, 084029
Sarzi, M., Shields, J. C., Schawinski, K., et al. 2010, MNRAS, 402, 2187
Savchenko, V., et al. 2017, GCN, 21507
Shabala, S. S., Ting, Y.-S., Kaviraj, S., et al. 2012, MNRAS, 423, 59
Singh, R., van de Ven, G., Jahnke, K., et al. 2013, A&A, 558, A43
Smartt, S. J., et al. 2017, Natur, https://doi.org/10.1038/nature24303
Stevenson, S., Berry, C. P. L., & Mandel, I. 2017, MNRAS, 471, 2801
Tanvir, N., & Levan 2017, GCN, 21544
Tanvir, N. R., Levan, A. J., Fruchter, A. S., et al. 2013, Natur, 500, 547
Tanvir, N. R., Levan, A. J., González-Fernández, C., et al. 2017, ApJL, https://doi.org/10.3847/2041-8213/aa90b6
Tauris, T., Kramer, M., Freire, P. C. C., et al. 2017, ApJ, 846, 170
Troja, E., Piro, L., van Eerten, H., et al. 2017, Natur, https://doi.org/10.1038/nature24290
van den Heuvel, E. P. J., Portegies Zwart, S. F., & de Mink, S. E. 2017, MNRAS, 471, 4256
von Kienlin, A., Meegan, C., & Goldstein, A. 2017, GCN, 21520
Yang, S., et al. 2017, GCN, 21531
Zevin, M., Pankow, C., Rodrigueiz, C. L., et al. 2017, ApJ, 846, 82